

## Article

# Particle Number and Size Distributions (PNSD) from a Hybrid Electric Vehicle (HEV) over Laboratory and Real Driving Emission Tests

Daisy Thomas<sup>1,2,\*</sup> , Hu Li<sup>1</sup> , Xin Wang<sup>3</sup> , Karl Ropkins<sup>4</sup> , Alison S. Tomlin<sup>1</sup> , Chris D. Bannister<sup>5</sup> and Gary Hawley<sup>5</sup>

<sup>1</sup> School of Chemical and Process Engineering, University of Leeds, Leeds LS2 9JT, UK

<sup>2</sup> 3DATX Corporation, 501 John James Audubon, Suite 200, Buffalo, NY 14228, USA

<sup>3</sup> School of Mechanical Engineering, Beijing Institute of Technology, Beijing 100081, China

<sup>4</sup> Institute of Transport Studies, University of Leeds, Leeds LS2 9JT, UK

<sup>5</sup> Institute for Advanced Automotive Propulsion Systems, University of Bath, Bath BA2 7AY, UK

\* Correspondence: daisythomas@3datx.com

**Abstract:** Particle number (PN) emissions from hybrid electric vehicles (HEV) during engine ignition and re-ignition events are an important but scarcely reported area. The objectives of the present work are to study the effects of drive cycle properties on the engine behaviour of a hybrid electric vehicle (HEV) and to investigate how this impacts the tailpipe PN emissions and their size distributions (PNSD). Worldwide harmonised light vehicles test cycle (WLTC) testing was conducted, as well as chassis dynamometer emission measurements over a realistic real driving emissions (RDE) speed pattern, using a Euro 5 Toyota Prius HEV with a Cambustion DMS500 sampling PN concentrations at the tailpipe. It is shown that the number of vehicle stops during a test cycle has a direct impact on the re-ignition activity for the HEV.  $64 \pm 3\%$  of the total PN from WLTC testing was produced during engine re-ignition events while only  $6 \pm 1\%$  was from stabilised engine operation. Similar proportions were observed for the RDE-style test cycle. The majority of engine reignition and destabilised activity, and hence PN emission, was during the low-speed sections of the drive cycles used. The average PNSD across cycle phases was different between cycles, due to the influence of dynamic properties on engine behaviour and hence the PN emission profile. The PNSD at the engine re-ignition and destabilised events had a merged wide peak with a maximum at 60 nm diameter and a shoulder at 12 nm diameter. The HEV had increased emissions of particles smaller than 23 nm under cold start, but similar overall PN emission values, compared to a warm start. The results of this work highlight the importance of controlling HEV PN emissions to limit human exposure to PN in urban environments where the majority of PN emissions occur. The sensitivity of HEV PN emission factors and PNSD to engine behaviour and, in turn, test cycle dynamic properties, is important to note when considering legislative test cycles, particularly with reference to the freedoms afforded by the RDE test cycle. The results also indicate that substantial improvements to air quality could be made by reducing the particle measurement protocol PN cut-off size to 10 nm.

**Keywords:** particle number; particle number size distribution; hybrid electric vehicle; drive cycle; WLTC; RDE



**Citation:** Thomas, D.; Li, H.; Wang, X.; Ropkins, K.; Tomlin, A.S.; Bannister, C.D.; Hawley, G. Particle Number and Size Distributions (PNSD) from a Hybrid Electric Vehicle (HEV) over Laboratory and Real Driving Emission Tests. *Atmosphere* **2022**, *13*, 1510. <https://doi.org/10.3390/atmos13091510>

Academic Editor: James Cizdziel

Received: 14 July 2022

Accepted: 10 September 2022

Published: 16 September 2022

**Publisher's Note:** MDPI stays neutral with regard to jurisdictional claims in published maps and institutional affiliations.



**Copyright:** © 2022 by the authors. Licensee MDPI, Basel, Switzerland. This article is an open access article distributed under the terms and conditions of the Creative Commons Attribution (CC BY) license (<https://creativecommons.org/licenses/by/4.0/>).

## 1. Introduction

Road transport is one of the major sources of particulate matter in urban environments. The size distribution of particulate matter coming from a vehicle exhaust depends on factors including engine type, fuel and exhaust after-treatment devices, in addition to the vehicle operating conditions and drive mode (normal/eco/sport), test method and atmospheric conditions at the time of measurement [1].

Though vehicle exhaust particulate emissions have historically been largely attributed to diesel engines, spark ignition (SI) engines can have a notable impact on particulate emissions and size distribution. The particle number size distribution (PNSD) from SI engines can be markedly different from diesel engines, in that the former generally has a unimodal distribution while the latter has a bimodal distribution [1]. The operating mode of an SI engine strongly affects the particle number (PN) and particle mass (PM) concentrations of the resulting particulate matter but does not seem to affect the PNSD [2]. The operating modes that contribute most strongly to particulate emissions are those associated with the enrichment of the fuel–air mixture. With the widespread application of particulate filters on diesel vehicles, the PN concentration from a state-of-the-art diesel vehicle could be lower than SI vehicles without a gasoline particulate filter (GPF). This highlights the necessity of more SI PN research [3,4].

For port fuel injection (PFI) SI engines, an enriched air–fuel mixture is needed during the cold start and warm-up phase to ensure enough fuel atomisation, proper ignition and smooth operation. This causes films of liquid fuel to accumulate on the combustion chamber walls, igniting capriciously and burning long into the expansion stroke [5]. Poor air–fuel mixing tends to increase the proportion of smaller particles, which means that, during a cold start, we are likely to see a larger distribution of smaller particles [6]. For harsh acceleration the same fuel enrichment may be applied [5]. Additionally, at high engine speed conditions, the exhaust temperatures can increase, so fuel enrichment may be used to protect the three-way catalyst (TWC) and other engine components from thermal stress [7]. A comparably high concentration of small particles can also be seen under high engine load conditions, attributed to the nucleation of exhaust-borne volatile and semi-volatile materials [3].

In addition to purposeful fuel enrichment, deviations away from stoichiometry can occur due to fuel being deposited on the inside of the intake port of PFI SI vehicles, rather than going into the combustion chamber. This is not a problem during steady-state operation as the oxygen sensor will allow this to be compensated for. However, during transient operation these reservoirs can be problematic as lean operation will be followed by rich operation due to improper fuelling management. When shifts in engine operation occur, the temperature of the inlet valve can change, altering the accumulation and evaporation of fuel reservoirs and hence the amount of soot seen at the tailpipe. Vehicles have additionally been seen to eject a large quantity of particulate matter as a result of the release of previously captured particles from the exhaust pipe walls [8].

Particulate matter from vehicle exhausts is considered one of the major sources of atmospheric particulate contamination [1]. The PNSD is an important factor to incorporate into considerations of particulate matter health risks because the ability of particles to penetrate deeply into human tissues depends on their size [9]. Particles with an aerodynamic diameter no larger than 10  $\mu\text{m}$  ( $\text{PM}_{10}$ ) or 2.5  $\mu\text{m}$  ( $\text{PM}_{2.5}$ ) are the most widely adopted index, as such particles are small enough to penetrate into the respiratory system [10]. It has been well recognized that  $\text{PM}_{2.5}$  gives a better indication of the health impacts as this size range can penetrate the deepest into the lungs [11]. Among  $\text{PM}_{2.5}$ , ultrafine particles with aerodynamic diameters of less than 100 nm are the most dangerous types [12]. This is due to smaller particles having much larger surface areas for toxic material adsorption, higher reactivity to induce inflammation [13,14] and long suspension times in the atmosphere.

Exhaust regulations were first introduced to monitor the mass emission rates of particulate emissions. However, PN became increasingly regarded as the exhaust particles became smaller but denser with the growing market share of direct injection SI engines. Smaller particles, with stronger penetration ability and related health hazards [1], contribute substantially less mass onto a filter, meaning that the gravimetric-based weighing methods for PM are approaching their technological limits for vehicles equipped with particulate filters [15]. As particulate measurement technologies have improved, the light-duty sector has been able to turn its focus to PN emissions. The Particle Measurement Programme (PMP) was launched in 2001 with the aim to develop a more sensitive and

precise measurement methodology for PN quantification, and in 2007 the solid particle number measurement method based on the counting of solid particles above 23 nm in size was introduced [16].

The nucleation of volatile fractions depends strongly on the condition of the exhaust dilution air and dilution ratio. As a result, the formation of particles smaller than 20 nm is heavily influenced by these conditions. The choice to count only solid particles greater than 23 nm was therefore made in the interest of measurement repeatability and reproducibility, because it is difficult to ensure that the exhaust sample conditions remain strictly constant [17]. The European Union (EU) solid particle number measurement method mandates a volatile particle remover upstream of a particle number counter with a 50% counting efficiency at 23 nm. This was integrated into the European light-duty automotive emission control regulations in 2009.

Previous research has focussed on the unique PN emission characteristics of hybrid electric vehicles (HEVs). Unlike internal combustion engine (ICE)-only vehicles, HEVs suffer extra PN penalties because the engine undergoes frequent stop-and-goes [18,19], though the aid of electric propulsion partially relieves PN deterioration during cold start compared to ICE-only vehicles [20,21]. More than two-fold higher than regulatory limit PN emissions were reported by Yang et al. [4] from a China-6 HEV during urban driving. Yang et al. [4] suggested that catalyst cooling during electric propulsion periods can be another factor resulting in extra PN when the engine restarts. Robinson and Holmén [19] also examined the PNSD from a 2010 model year/SULEV-II HEV and found a bi-modal distribution with peaks at 50 and 400 nm, while the 10 nm peak visible from an ICE-only counterpart was not evident. Driven by the global efforts to decarbonise and reduce emissions, HEVs—together with electric vehicles—are quickly replacing ICE-only models in mainstream markets. This makes it all the more important to better understand PN emissions and their size distribution from HEVs. The New European Drive Cycle (NEDC) that was used for type approval in the EU from Euro 3 until Euro 6 emission standards was replaced by the Worldwide Harmonised Light Vehicle Test Procedure (WLTP) and Worldwide Harmonised Light Vehicle Test Cycle (WLTC) because the NEDC was deemed unrepresentative of “real-world” driving and too easy to manipulate [22]. More recently, a supplementary on-road test called the real driving emissions (RDE) test was added alongside the WLTC as a means to protect against so-called “cycle beating” on the fixed chassis dynamometer test cycles that led to the “Dieselgate” scandal of 2015 [23].

Robinson and Holmén [19] inferred from their on-road city driving investigation that the PN size distribution changes little over the route for a given vehicle type. However, no work to date has directly investigated how the type approval test cycles affect the PN and PNSD arising from an HEV. Given that many HEVs have been shown to display different PN emissions from conventional vehicles, it is important to assess how the test cycles used at type approval affect this.

The objective of the current study is to investigate the PN and PNSD arising from an HEV on the WLTC and an RDE-style chassis dynamometer test cycle. By assessing how the properties of these test cycles affect the PN and PNSD from HEVs, inferences can be made as to how the reported PN results are affected by the test cycle used.

## 2. Materials and Methods

### 2.1. Test Vehicle, On-Board Instrumentation and Fuel

A 2010 model year Third Generation Toyota Prius with Euro 5 emission compliance and 26,000 miles on the odometer was used for this study. This test vehicle and its onboard instrumentation are already detailed in Thomas et al. [24] and so will only be briefly outlined here. Table 1 summarises the properties of the test vehicle. A feature of this and other HEVs is their stop-and-go functionality whereby the ICE turns off when the vehicle is at standstill and re-ignites when the accelerator pedal is depressed. This ICE re-ignition is referred to as “engine re-ignition” in this paper. A range of thermocouples placed around the TWC system and at the tailpipe measured associated temperatures, while an OBD

Mini Logger (HEM Data, Southfield, MI, USA) recorded a range of engine control unit (ECU) parameters, including lambda, mass air flow, engine coolant temperature and hybrid battery state of charge (SOC). A Horiba OBS-1000 (Horiba, Kyoto, Japan) also measured the air–fuel ratio downstream of the muffler.

**Table 1.** Properties of the HEV research vehicle.

Engine capacity (Litres, L)	1.8
Engine maximum power (kilowatts, kW)	73
Motor maximum power (kW)	60
Injection	PFI
Transmission	E-CVT
Curb weight (kilograms, kg)	1380
Aspiration	NA
Engine cycle	Atkinson
Compression ratio	13
Exhaust gas recirculation (EGR)	Yes
Turbocharged/supercharged	No

PFI: port fuel injection; E-CVT: continuously variable transmission using a planetary-gear energy distributor; NA: naturally aspirated.

The fuel used was an E10 blend. Ethanol was splash blended into research grade E0 gasoline to make a 10% by volume ratio. For the fuel change, the entire tank was first drained as fully as possible by a fuel pump attached to a connection in the fuel return line under the vehicle bonnet. Approximately 2 L of the new fuel was then poured into the fuel tank. This process was repeated with the drained fuel from each iteration being deposited in a waste fuel container. The process was repeated at least three times to ensure the tank and fuel delivery lines were flushed before the desired quantity of fuel for testing was added. After this, the vehicle was driven approximately 50 km on the chassis dynamometer, ensuring that the new fuel had completely flushed out the old fuel and that the ECU had adjusted to the different combustion properties of the new fuel type.

## 2.2. Chassis Dynamometer Test Cell

The University of Bath Centre for Low Emissions Vehicle Research (CLEVeR) (Bath, UK) chassis dynamometer test cell was used for this project. The tests were performed on a 4WD AVL RoadSimTM 48" chassis dynamometer (AVL, Graz, Austria) with a Horiba CVS-7100 system (Horiba, Kyoto, Japan), within a test cell capable of temperature and humidity control. A near full-frontal width road speed fan was placed approximately one metre in front of the vehicle for representative cooling of the full powertrain system. A Cambustion DMS500 fast particle size spectrometer (Cambustion, Cambridge, UK) was placed at the tailpipe for PN and PNSD measurement at 5 Hz sampling frequency. The Horiba smooth approach orifice and CO<sub>2</sub> tracer capability each also enabled exhaust flow determination and hence transient tailpipe emission calculation.

## 2.3. Test Procedure and Test Cycles

All tests were driven by the same trained test driver. The chassis dynamometer was warmed up according to the manufacturer's instructions at the beginning of each day of testing. The various pieces of equipment were turned on and any preparations for testing were performed as necessary, according to user manuals.

The WLTC cycle was performed largely according to the guidelines in Commission Regulation (EC) 2017/1151 [25]. The main exception to this was the absence of any volatile particle remover and no cut-off at 23 nm ahead of the particle number counter, to allow more detailed characterisation of the particulate matter. The WLTC speed profile is presented in

Figure 1. The WLTC test was repeated two times under identical initial hybrid vehicle SOC of 67.8%, to ensure reliability. A third WLTC test was also performed, but with a warm engine (starting engine coolant temperature 57 °C; initial SOC 68.2%) in order to allow the investigation of the cold start effect on PNSD.

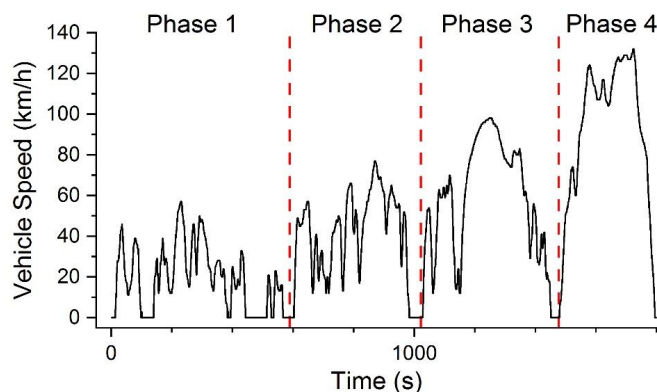


Figure 1. Speed profile of the WLTC.

Due to bag sampling constraints, a full RDE cycle could not be performed on the chassis dynamometer. The volumetric capacity of the bag sampling system did not allow for such a large test. Instead, a “shortened RDE-style cycle” was executed on the chassis dynamometer. The shortened RDE-style cycle was a real-world velocity trace of an on-road test-driven in and around the city of Leeds, United Kingdom (UK), using the same research vehicle. The test—of 36.09 km distance and 2310 s duration—gave rise to the velocity trace given in Figure 2a. This was then transposed into the test cell driver’s aid and driven on the chassis dynamometer according to the limits defined for the WLTC driver’s schedule. The shortened RDE-style drive cycle was repeated 3 times on the dynamometer with varying initial hybrid batteries SOC values (52.2%, 60% and 67.8%). The initial coolant temperatures for these three tests were  $53 \pm 8$  °C.

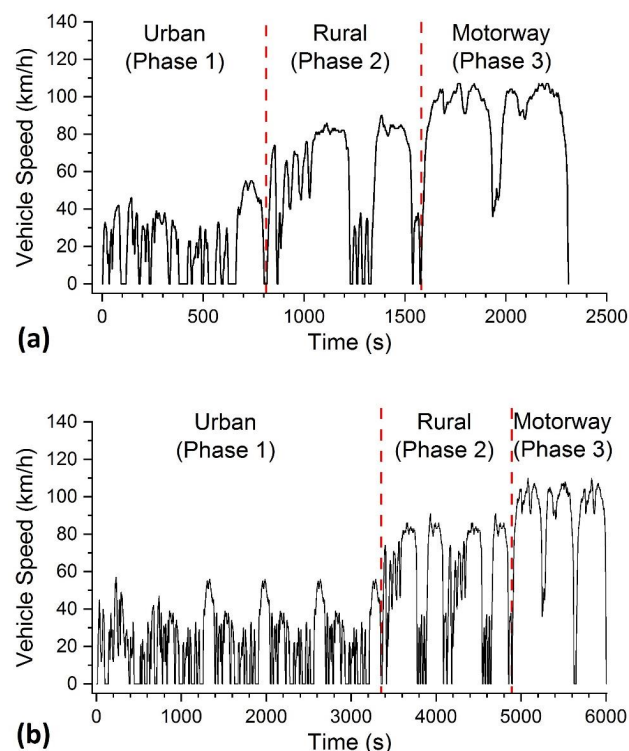


Figure 2. (a) Speed profiles of the shortened RDE-style chassis dynamometer drive cycle and (b) full RDE-style drive.

A composite “RDE-style cycle” was then created to allow cycle-average PNSD comparisons of an RDE cycle to be made against the WLTC. To do this, sections of the shortened RDE-style cycle were repeated in post-processing to build up a full-length RDE cycle. The shortened RDE-style cycle driven on the chassis dynamometer was from a warm start, and so phase 1 of the WLTC was incorporated into the beginning of the composite RDE-style test cycle to make it a cold start test. The resulting test cycle satisfied all of the dynamic requirements of the RDE package 4, as well as being within the moving averaging window tolerance (based on the CO<sub>2</sub> characteristic curve values resulting from the average of the legislative WLTC tests described above). The original speed profile of the shortened RDE-style cycle driven on the chassis dynamometer is given in Figure 2a and the RDE-style cycle from which cycle-average PNSD values were attained is given in Figure 2b. The urban, rural and motorway sections are referred to as “phase 1”, “phase 2” and “phase 3” respectively throughout this paper, unless otherwise stated.

Properties of the composite RDE-style cycle and the WLTC cycle are given in Table 2. To enable easy comparison between tests the characterisations of “urban”, “rural” and “motorway” are used in Table 2 for both WLTC and RDE, according to the definitions of the RDE legislation:

- Urban: vehicle speed  $\leq 60$  km/h,
- Rural:  $60$  km/h  $<$  vehicle speed  $\leq 90$  km/h,
- Motorway: vehicle speed  $> 90$  km/h.

**Table 2.** Properties of the WLTC and RDE-style cycles.

	WLTC	RDE
Urban distance (kilometres, km)	8.588	25.66
Rural distance (km)	5.788	22.27
Motorway distance (km)	8.398	23.81
Urban percent distance (%)	37.71	35.77
Rural percent distance (%)	25.42	31.04
Motorway percent distance (%)	36.87	33.19
Total distance (km)	23.27	72.67
Stoppage percent time (%) *	20.34	24.85
Average number of stops per km (#/km) *	0.43	0.92
Maximum speed (km/h)	131	110
Time over 100km/h velocity (s)	181	454
Total time (min)	30	99.98
Cold start time (s)	300	300
Cold start stoppage time (s) *	55	55
Urban percent time accelerating (%)	79	44
Rural percent time accelerating (%)	28	23
Motorway percent time accelerating (%)	13	25
Urban $v_{a_{pos}}(95)$ ** ( $m^2/s^3$ )	11.30	8.93
Rural $v_{a_{pos}}(95)$ ( $m^2/s^3$ )	13.15	12.42
Motorway $v_{a_{pos}}(95)$ ( $m^2/s^3$ )	13.66	7.74
Urban RPA *** ( $m/s^2$ )	0.50	0.47
Rural RPA ( $m/s^2$ )	0.29	0.26
Motorway RPA ( $m/s^2$ )	0.23	0.16
Urban average speed (km/h)	25.98	22.77
Rural average speed (km/h)	73.27	78.90
Motorway average speed (km/h)	110.74	100.26

\* In this table “stop” refers to a vehicle velocity of less than 1 km/h. \*\*  $v_{a_{pos}}(95)$ : the 95 percentile of the products of vehicle speed and positive acceleration in each RDE stage, is a metric introduced in Euro-6 RDE regulation to prevent overly aggressive driving style that may induce artificially high emissions. \*\*\* RPA: relative positive acceleration, is a metric introduced in Euro-6 RDE regulation to prevent overly gentle driving style which may induce artificially good emission results.

#### 2.4. Data Processing

The chassis dynamometer test cell in-house equipment was automatically time aligned. The data from the ECU was aligned to this via matching of the exhaust flow rates calculated for each (and checked by comparing vehicle velocity traces). The Horiba OBS-1000 was then aligned to these using the exhaust flow rate measurement. The thermocouple exhaust temperatures and DMS500 PN values were aligned to the engine speed (RPM) from the ECU, matching signal increases for both the engine start and engine restart events, as indicated by the RPM signal.

The emission rates of the DMS500 particle number (#/s) were calculated as the product of the number concentration and the tailpipe exhaust flow rate. The size-distributed concentration values were first converted to size-distributed PN emission rates. The data was then categorised into four engine-mode operations. “Engine off” was categorised as any portion of time with engine speed below 500 rpm. “Engine re-ignition event” was categorised as the four seconds with engine speed higher than 500 rpm after a period in “engine off” mode. “Engine stabilised” was categorised as any period of engine speed above 800 rpm that was more than 10 s from an engine speed lower than 500 rpm. “Engine destabilised” represented all other engine states, i.e., any period 5–10 s after engine ignition or re-ignition and the 10 s before an engine off event, or any other period with engine speed between 500–800 rpm.

### 3. Results and Discussion

#### 3.1. Drive Cycle Property Impact on Engine Behaviour

The dynamic properties of the drive cycles outlined in Table 2 have a large impact on the engine behaviour of the hybrid research vehicle. Building on the work of Conger and Holmén [26], the time and distance occupied by different HEV operating states were calculated. The percentage distribution of the different engine states with respect to time and distance for each phase of the RDE-style and WLTC cycles are given in Figures 3 and 4, respectively. The number of vehicle stops during a drive cycle has a direct impact on the percentage of time and distance covered with the engine in a state of re-ignition. The cycle dynamic properties also affect the number of individual engine restart events over the course of the test cycle, and these are given in Figure 5 for individual cycle phases and for the total cycle. As the RDE was based on a real-world test drive, the number of stops per kilometre was not the same as the WLTC cycle. The following section will investigate the effect that this has on PN emission factors.

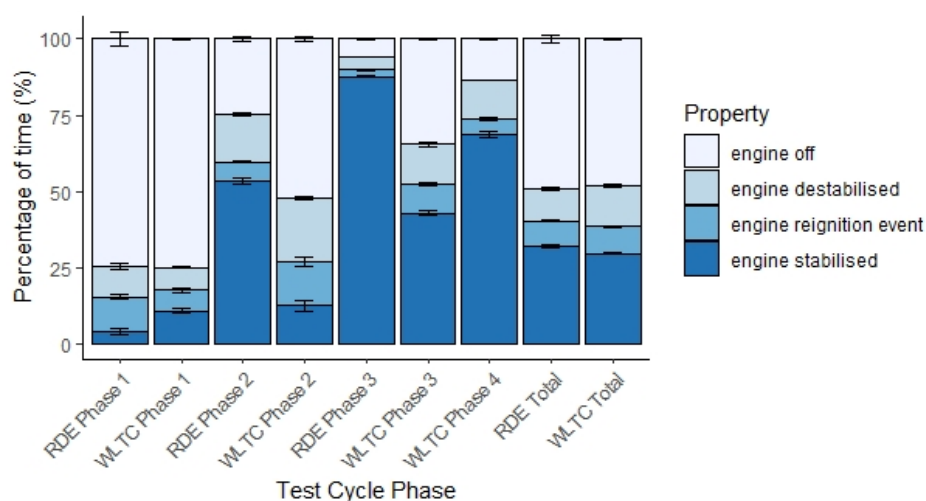


**Figure 3.** Percentage of time covered with the engine in different states of operation. Error bars represent the standard error of the repeats (two tests for each WLTC phase, three tests for each RDE phase).

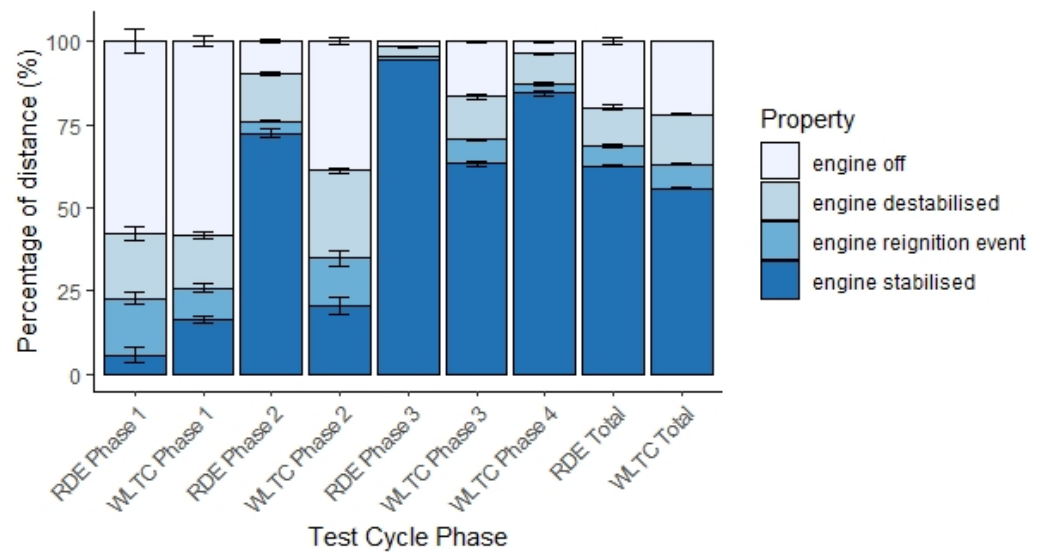


**Figure 4.** Percentage of distance covered with the engine in different states of operation. Error bars represent the standard error of the repeats (two tests for each WLTC phase, three tests for each RDE phase).

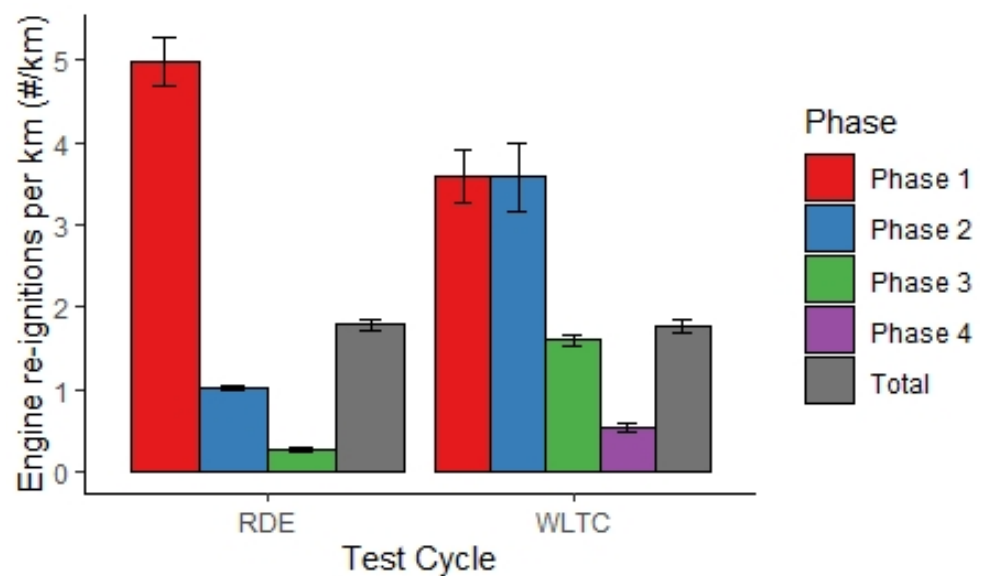


**Figure 5.** Number of engine re-ignition events per km for the total WLTC and RDE-style test cycles and their individual phases. RDE phases are called phase 1 (urban), phase 2 (rural) and phase 3 (motorway) for comparison with the WLTC cycle phases. Error bars represent the standard error of the repeats (two tests for WLTC, three tests for RDE).

With regard to the differences between Figures 3 and 4, it is clear that when properties are represented as a percentage of distance, rather than time, the stabilised engine operation increases in proportion while the engine off decreases in proportion. The engine destabilised and re-ignition event proportions increase for lower velocity phases 1 and 2 but decrease for higher velocity phase 3 and (WLTC) phase 4. These trends occur because the type of driving under which the engine is in flux between being on and off generally occurs at low but non-negligible speeds. The average speed of the re-ignition events across cycles was  $38.3 \pm 0.1$  km/h for WLTC and  $31 \pm 1$  km/h for RDE.

### 3.2. Total PN

The average PN emission factors for each phase of the RDE-style and WLTC cycle, and for the total test cycles, are given in Figure 6. The overall PN emission factors for both RDE and WLTC testing are  $7.3 \times 10^{11}$  #/km and  $1 \times 10^{12}$  #/km, respectively; above the Euro 6 limit of  $6 \times 10^{11}$  #/km for this Euro 5 HEV. The urban section of the RDE test gave a PN emission factor of  $1.8 \times 10^{12}$  #/km; above the current RDE not-to-exceed (NTE) limit of  $9 \times 10^{11}$  #/km (1.5 times the Euro 6 limit). It should be noted that the PN emissions in Figure 6 represent volatile and non-volatile particles with a size range of 5–1000 nm, while the EU PN limit is for non-volatile particles with a size range of 23–560 nm. Nevertheless, the magnitude of exceedance is notable, and indicates that PFI HEV PN emissions should be more carefully monitored and considered in future regulations. Yang et al. [4] also found that their PFI HEV exceeded the RDE not-to-exceed (NTE) limit of  $9 \times 10^{11}$  #/km when conducting RDE testing. Their PFI HEV results were even higher than those of a conventional GDI vehicle with no GPF. Yang et al. [4] similarly concluded that PN emissions of PFI HEVs should not be overlooked.

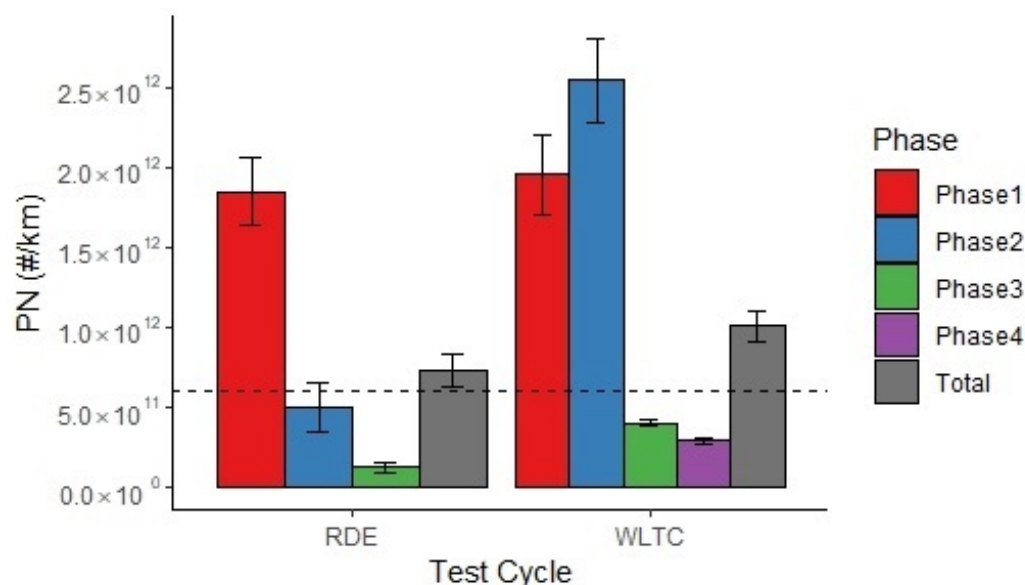


**Figure 6.** Average PN emissions per kilometre across the WLTC and RDE test cycles. Individual phase and total cycle results are given, along with the Euro 6 PN limit of  $6 \times 10^{11}$  #/km (dotted line). Error bars represent the standard error of the repeats (two tests for WLTC, three tests for RDE).

By comparison with Figure 5, it can be seen from Figure 6 that the total PN emitted is related to the number of engine restarts per kilometre. Indeed, Figure 7a,b show that for both WLTC and RDE, there are significant PN emissions associated with engine re-ignition events. Figure 8 confirms a strong positive correlation between the number of engine restarts per kilometre of a drive section and the resultant PN emission factor for that section. For the tests under study,  $64 \pm 3\%$  of total PN for WLTC and  $77 \pm 4\%$  of total PN for RDE was produced during engine re-ignition events, and  $30 \pm 4\%$  and  $13 \pm 1\%$  was produced during engine destabilised operation for WLTC and RDE, respectively, while  $6 \pm 1\%$  and  $10 \pm 3\%$  was from stabilised engine operation for WLTC and RDE, respectively. Therefore, the dynamics of a drive cycle have a very large effect on the PN emission factors that result for HEVs: the greater the number of stops per km on the cycle, the greater the PN emission factors. Compared to the regulatory PN limit for both laboratory and real driving emissions, the PN issue of HEVs is dominated by urban driving. Considering public exposure, controlling PN emissions from HEVs in urban areas requires more attention.

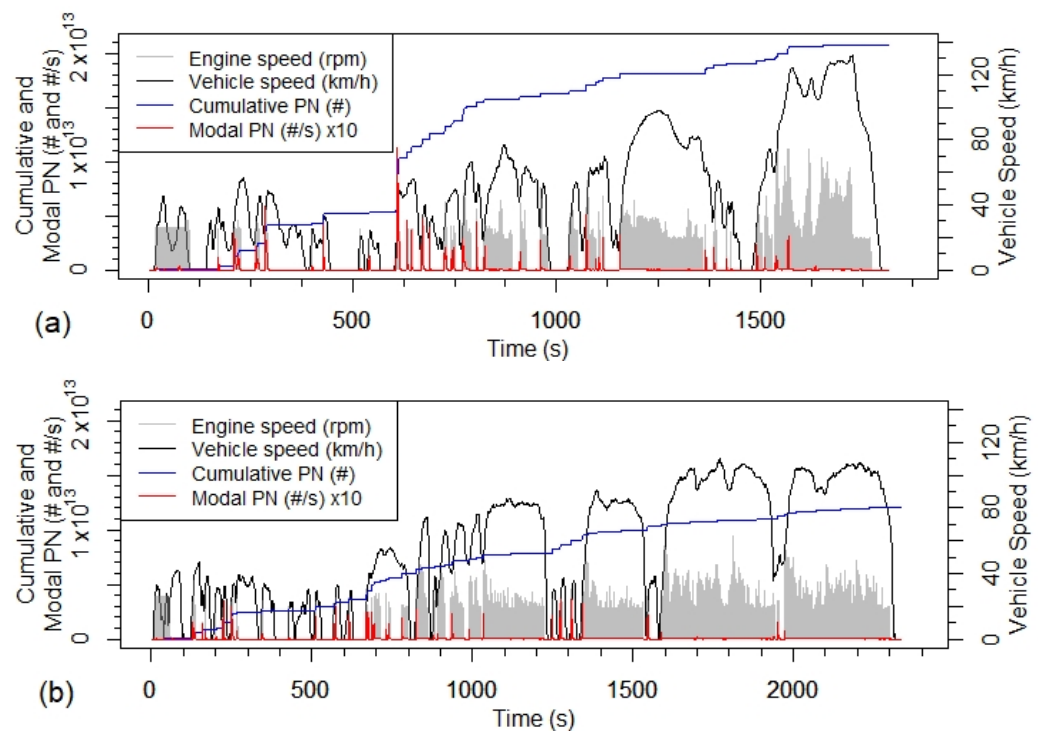


**Figure 7.** Modal (i.e., transient) and cumulative PN emissions over (a) the WLTC and (b) the shortened RDE-style cycle. Transient values are multiplied by 10 for scale. Vehicle speed is indicated on the secondary axis, with engine RPM indicated qualitatively in grey.

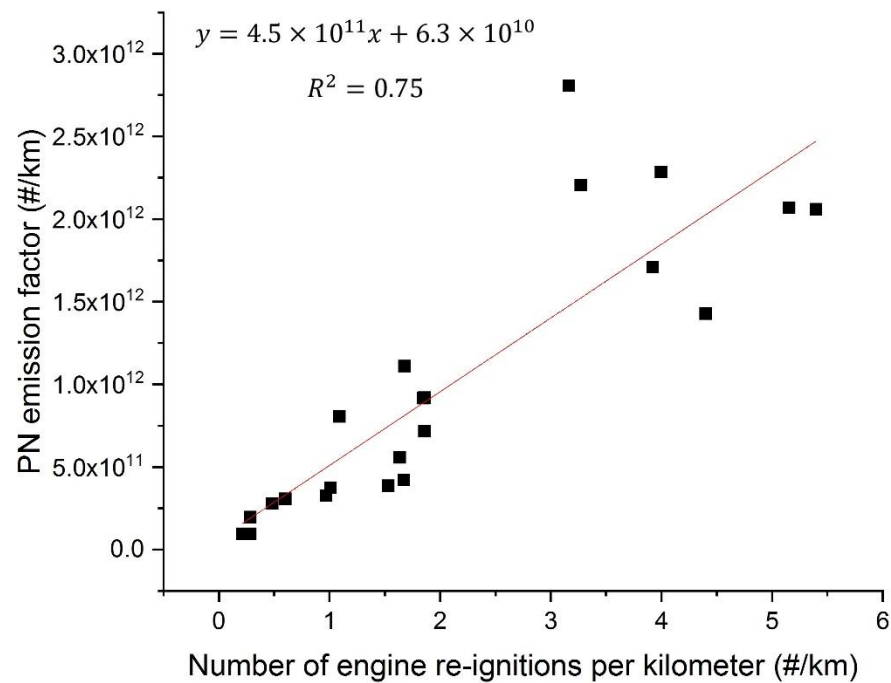


**Figure 8.** HEV PN emission factor versus the number of engine re-ignition events per kilometre.

### 3.3. PNSD

The time-averaged PNSDs across the WLTC and RDE cycles are given in Figures 9 and 10, respectively. One can see a rather different PNSD arising from the RDE compared to the WLTC.

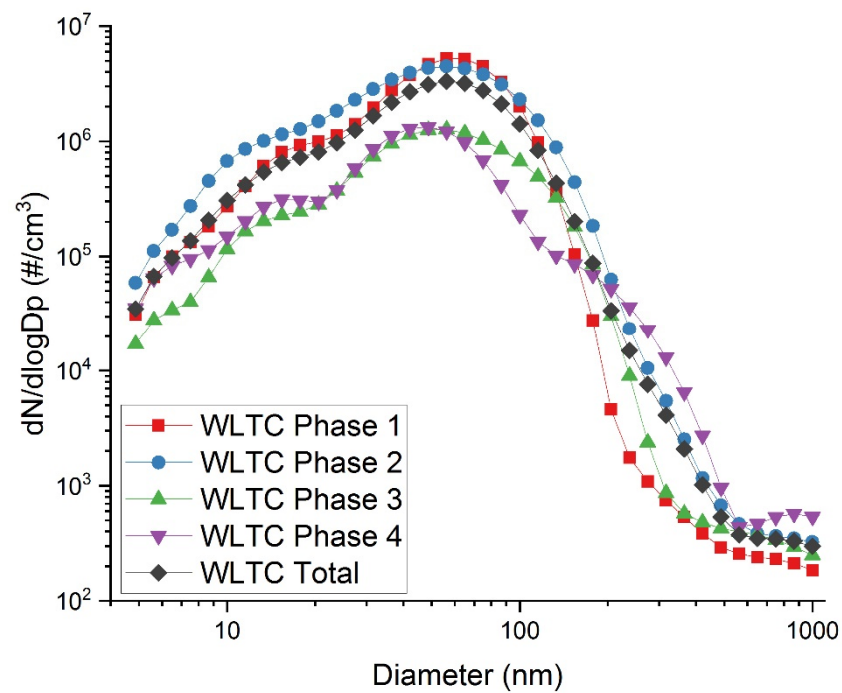


Figure 9. WLTC total and phased average PNSD.

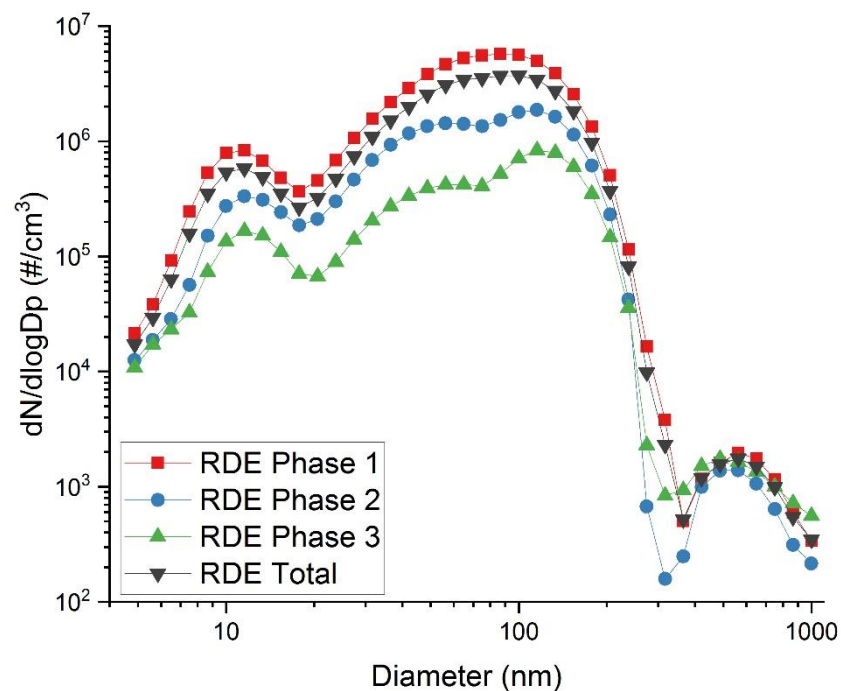
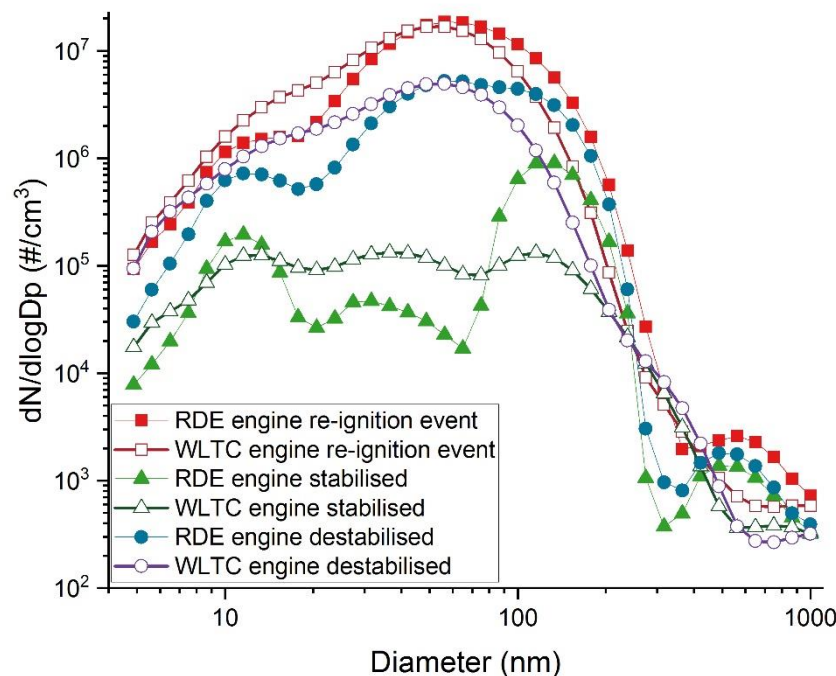


Figure 10. RDE total and phased average PNSD.

The reason for these differences is due to the variation in PN emissions seen under different types of engine operation, displayed in Figure 11. Whilst the engine is undergoing a re-ignition event (the 4 s following engine re-ignition) the PNSD showed overlapping between two modes (60 nm and 12 nm particle diameter), i.e., the distributions at 60 nm and 12 nm were getting wider. When the engine is under stable engine operation (at least 10 s after any engine start and 10 s before any engine off), a tri-modal average PNSD is seen, with local maxima at 12 nm, 35 nm and 115 nm. The destabilised engine operation has a broadly similar shape to the engine re-ignition state, as it is mainly caused by the same mechanisms. Delayed PN spikes on engine re-ignition sometimes cause the PN emission

event to exceed the 4 s limit for the “engine re-ignition state” and cross over into the destabilised state. Sudden increases in engine speed either soon after the engine reignited, or soon before the engine turned off, also cause PN emissions during these destabilised engine states.

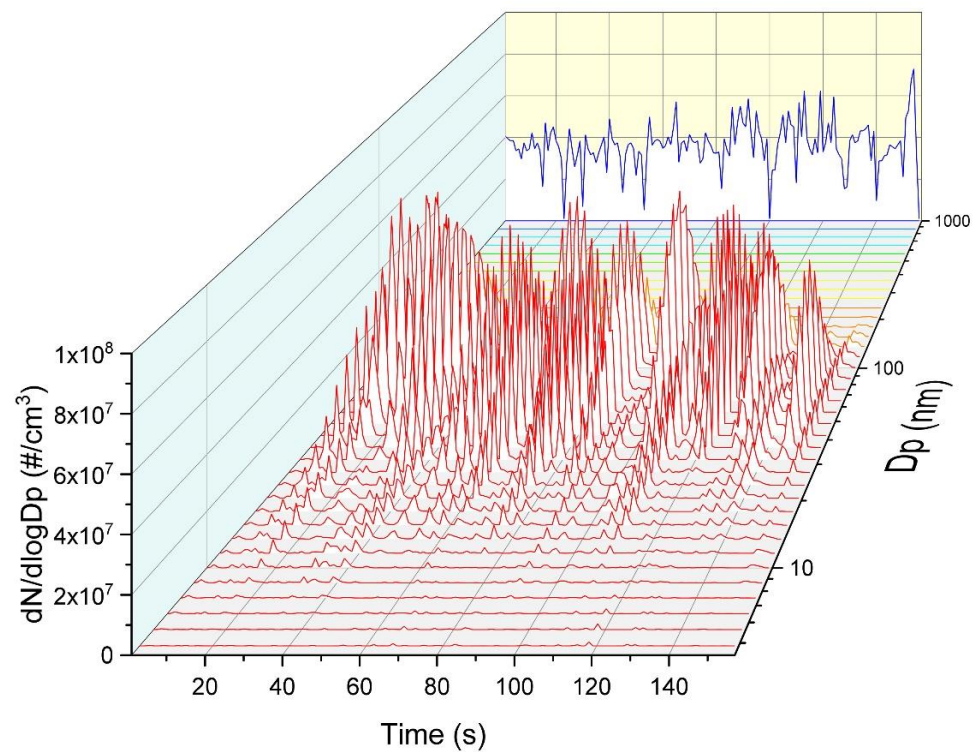


**Figure 11.** Average WLTC and RDE PNSD during engine re-ignition event, engine stabilised and engine destabilised states.

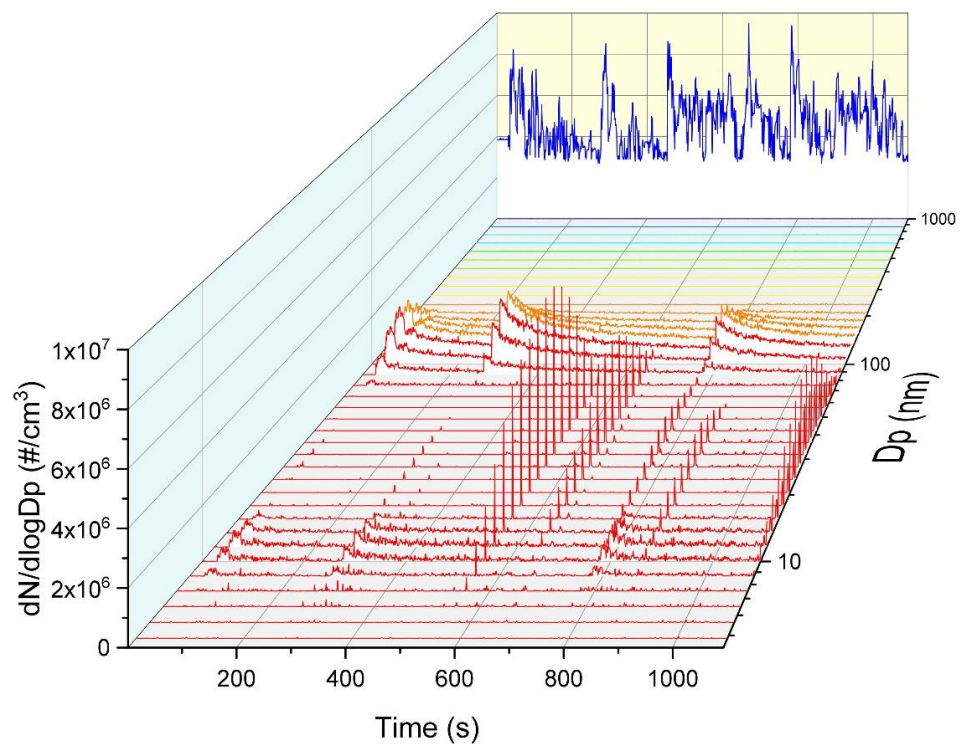
Consideration of the re-ignition events illustrated in Figure 12 and the stable engine operation illustrated in Figure 13 confirms that the re-ignition events have a merged wide distribution with a maximum at around 60 nm particle diameter. Meanwhile, the stable engine operation regions have two almost-constant magnitude, low-concentration peaks with maxima at 12 nm and 115 nm, and intermittent high magnitude peaks at 35 nm associated with sudden increases in engine speed. The 12 nm and 115 nm mode PN peaks visible during stabilised engine activity are thought to be a product of combustion and are produced throughout all engine combustion activity. These modes appear visually enveloped and engulfed by the high-concentration broad PNSD of the re-ignition event PN spikes. The 12 nm particles may also coagulate and adsorb onto the larger particles produced during the high PN concentration engine re-ignition events, thereby reducing the concentration in that size range. The 12 nm mode PN at the stable engine operation region could be due to the contribution from lubricating oil. Premnath et al. [27] reported that engine lubricating oil can have an influence on solid particle number in the sub-23 nm size range, particularly the contribution from ash or metal additives. There are small peaks for particles around 115 nm immediately following a PN emission spike, which gradually decline through time. These could be due to the re-entrainment and resuspension of the particles that had deposited on the inner surfaces of the tailpipe when the RPM and engine load suddenly increased.

These different modes are the origin of the different PNSDs seen in Figure 11. This is because, as discussed in Section 2.2, these WLTC and RDE cycles have different dynamic properties, so the proportions of these types of engine behaviour are different, and therefore the PNSD is different. The WLTC is more transient than this example RDE cycle (visible in the properties of Table 1), and therefore the engine undergoes more re-ignitions and changes in speed. This increases the “engine re-ignition event” PN emissions in the

35–60 nm region and leaves proportionately lower “engine stabilised” PN emissions at 12 nm and 115 nm.

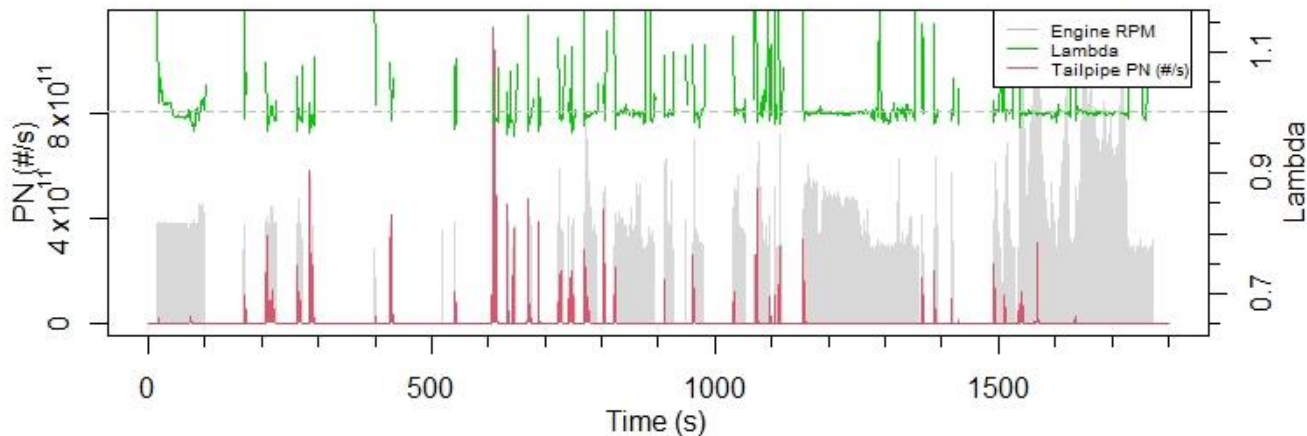


**Figure 12.** Example of one RDE test PNSD with time for all engine re-ignition events. Engine RPM is indicated in blue at  $3 \times 10^4$  times scale.



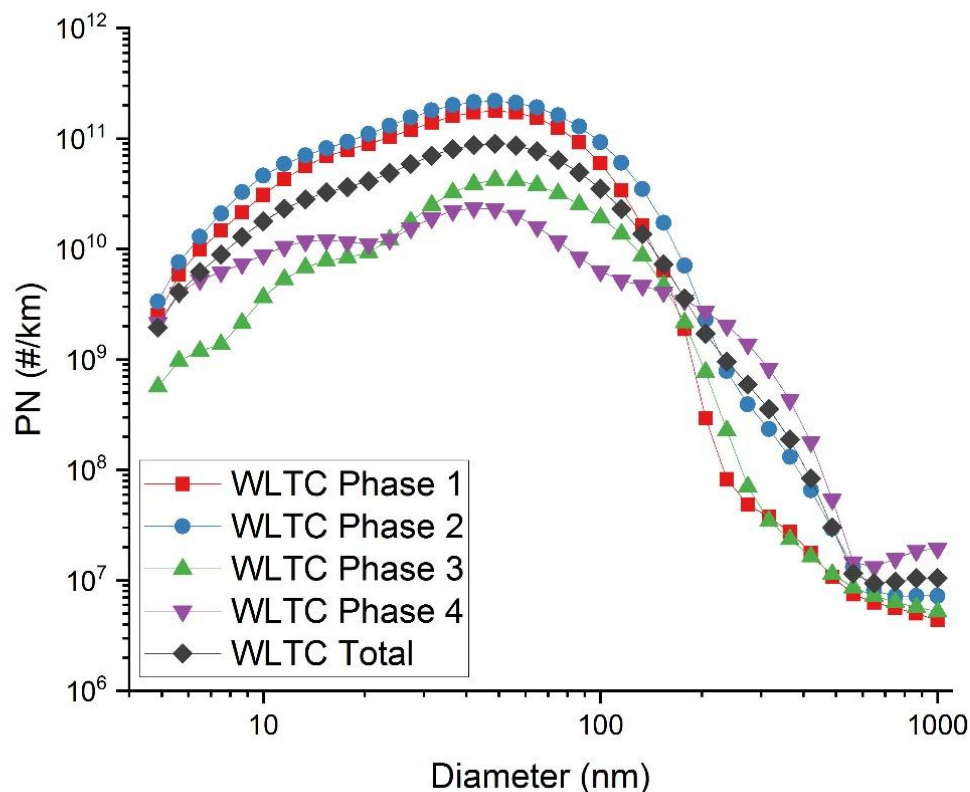
**Figure 13.** Example of one RDE test PNSD with time for all engine stabilised operation. Engine RPM is indicated in blue at  $3 \times 10^3$  times scale.

Figure 14 shows that the re-ignition PN spikes with a maximum number concentration at a diameter of approximately 60 nm are associated with fuel enrichment events, likely a strategy utilised by this vehicle to ensure good combustion on engine ignition. This is in agreement with the findings of Conger and Holmén [26].



**Figure 14.** Total HEV PN emission rate alongside engine RPM and lambda (the actual air–fuel ratio divided by the stoichiometric air–fuel ratio).

Figures 15 and 16 show the distance-specific PNSDs. The resulting patterns are similar to the time-averaged PNSD concentration values in Figures 9 and 10.



**Figure 15.** Average size distributed PN emission factors from individual phases and total WLTC cycles.

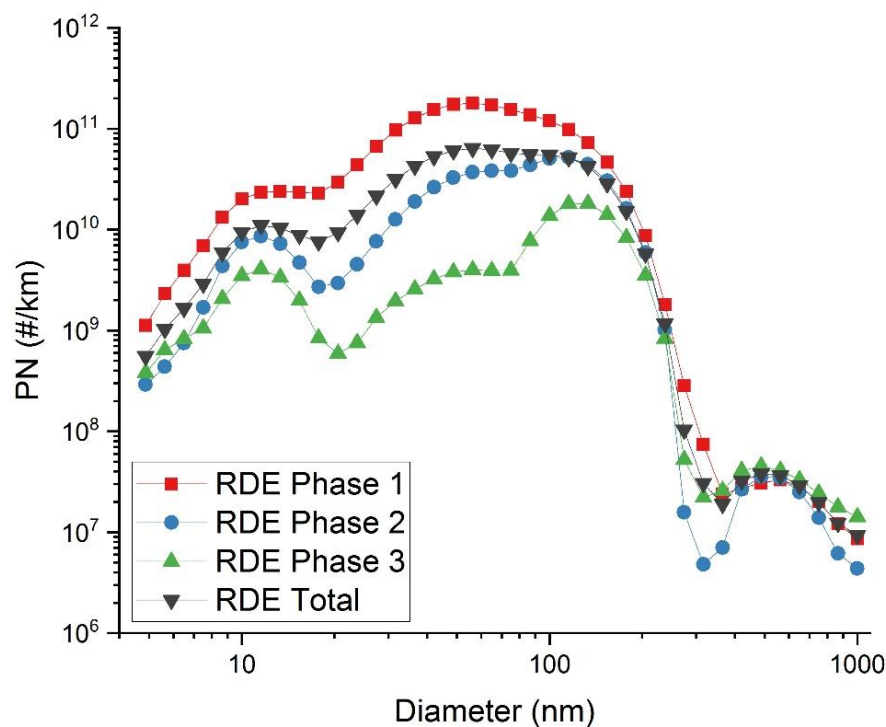


Figure 16. Average size distributed PN emission factors from individual phases and total RDE cycles.

3.4. Cold Start PNSD

The WLTC was repeated under warm engine conditions, and Figure 17 displays the average PNSD from the first 300 s of this cycle, compared to two repeats of the cold start WLTC. There is clearly some difference, with the cold start cycles having a broader maximum that encompasses the 12–60 nm region, while the warm start cycle has a more distinct maximum at 60 nm and shoulder at 12 nm. This behaviour was observed under multiple tests.

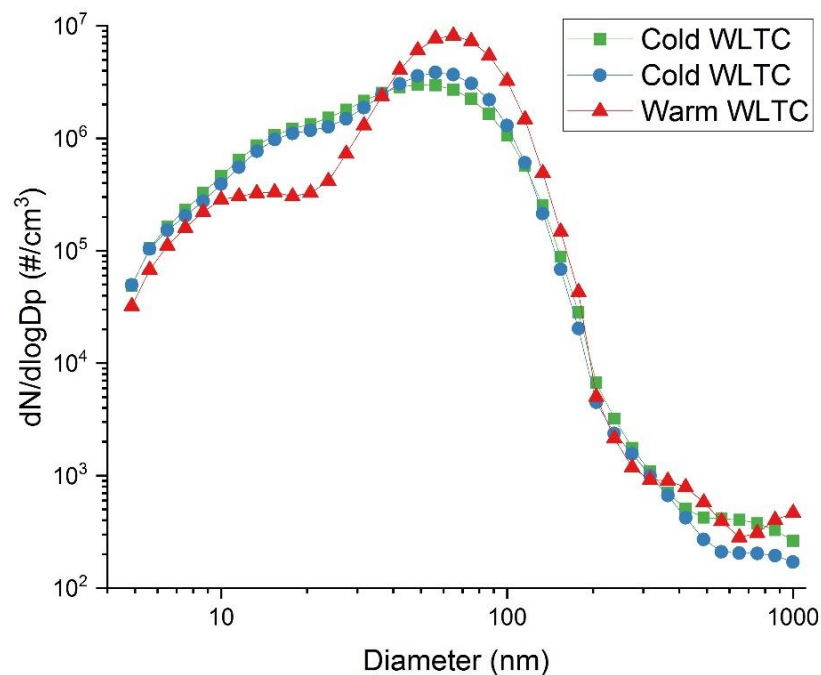
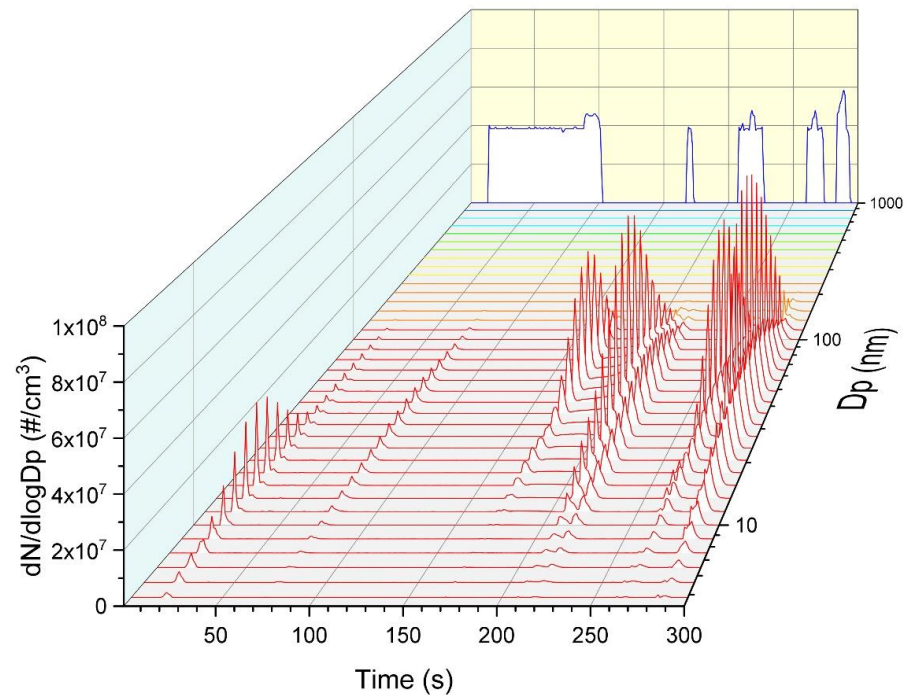
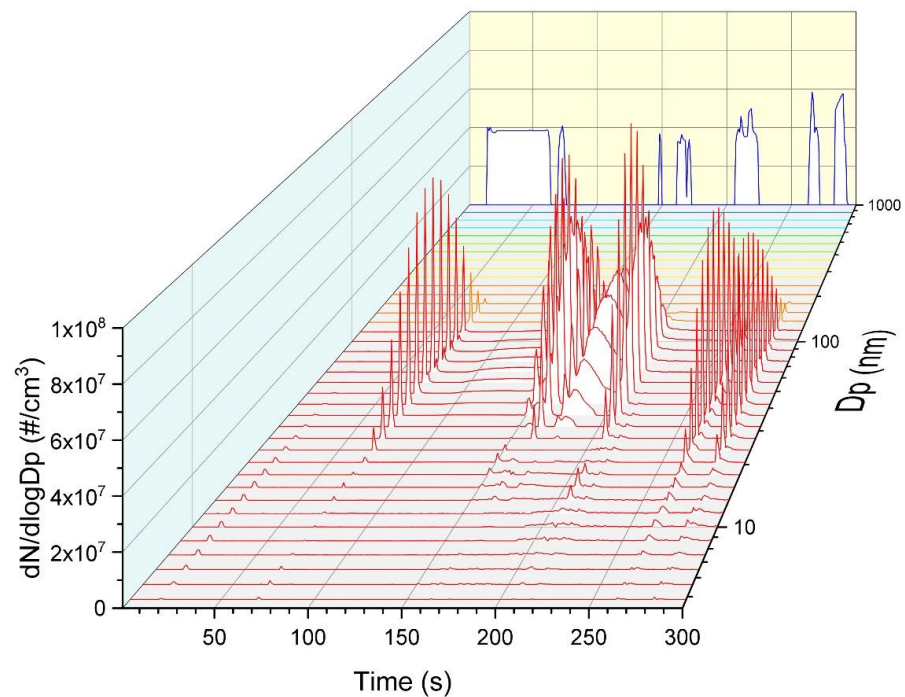


Figure 17. Comparison of the average PNSD over the first 300 s of cold and warm start WLTCs.

Figure 18 shows the transient PNSD from the first 300 s of one cold start WLTC. The initial engine ignition PN event has a maximum at 12 nm and is the cause of the extended maximum seen for the cold start tests in Figure 17. For the warm start test in Figure 19, the initial engine ignition only causes a very small PN emission event at this diameter, hence the shoulder seen.



**Figure 18.** Transient PNSD over the first 300 s of a cold start WLTC. Engine RPM is indicated qualitatively in blue on the back wall.



**Figure 19.** Transient PNSD over the first 300 s of a warm start WLTC. Engine RPM is indicated qualitatively in blue on the back wall.

The smallest particles are likely to be unburnt fuel fractions arising from the inhomogeneous, incomplete combustion of rich air–fuel mixtures within the cold combustion chamber and metal-containing particles derived from lubricating oil [5,6]. After the initial start-up, any subsequent engine activity occurs within a hot combustion chamber, so the fuel is fully vaporised. The fuel enrichment conditions on engine restart can still lead to soot, which is generally of the larger sizes visible throughout the rest of the test [5].

Most of this cold start spike would not be captured by a 23 nm cut-off, as per the current legislation for WLTC and RDE testing. Should this cut-off diameter be reduced to 10 nm, however, then this spike would be represented in the emission results provided that it is composed of any solid particles, which has previously been demonstrated by Giechaskiel et al. [28]. It is also worth noting that this HEV does not suffer from increased PN emissions during cold start compared to warm engine operation, visible by the similar magnitude of PN emissions in Figure 17.

### 3.5. Effect of the 23 nm PN Size Cut-Off

As discussed in Section 1, the type approval legislation currently sets a lower limit of 23 nm diameter to the size of PN counted [28]. However, legislators are currently debating the possibility of lowering this limit to diameters such as 10 nm in order to capture more of the harmful nanoparticles that can cause worse damage when inhaled. In order to study the effect that this would have on the PN emission results, the WLTC and shortened RDE-style tests have had their  $PN_{23nm}$ ,  $PN_{10nm}$  and  $PN_{5nm}$  estimated from size-distributed DMS500 data. The results for the WLTC and shortened RDE-style tests are displayed in Figure 20 a and b, respectively. For comparability to the RDE cycle, the WLTC cycle has been divided into urban (WLTC phase 1), rural (WLTC phases 2 and 3) and motorway (WLTC phase 4) sections. For the whole WLTC cycle, the PN emission results going from a cut-off of 23 nm to 10 nm increased by 25% and from a cut-off of 23 nm to “total” (4.87 nm) PN increased by 31%. These differences are much smaller than those witnessed for two PFI SI vehicles on the NEDC and WLTC test cycles by Giechaskiel et al. [28], indicating that HEVs utilising PFI technology cannot be assumed to have the same PN size distribution characteristics as their conventional ICE counterparts. For the WLTC urban section, the increases were similar to the total, standing at 26.5% and 30.7%, respectively. For the shortened RDE-style cycle, PN emission results increased by 9.7% going from 23 nm to 10 nm, and 12.1% going from 23 nm to total PN. For the urban section specifically, the increase was similar to that of the total test, standing at 8.7% and 10.5%, respectively. There are differences between values for the different test cycles, and this is mainly due to the fact the WLTC was from a cold start, while the RDE-style cycle was from a warm start. The proportion of sub 23 nm particles is larger under cold start conditions.

It is clear that a lowering of the cut-off size would increase the reported PN emission results at type approval. This would force car manufacturers to take more action to limit tailpipe PN emissions in order to ensure that their vehicles pass the tests, and thus help to lower PN air pollution levels. The majority of the difference in emissions is achieved by reducing the cut-off to 10 nm. It is a challenge to accurately and reliably measure the smaller nanoparticles. By comparison with Giechaskiel et al. [28], it can be inferred that if PFI vehicles are also made subject to the PN emission regulations, and the size cut-off is reduced from 23 nm to 10 nm, then HEV PFI vehicles would see a smaller percentage increase in reported PN emissions as a result, than conventional PFI vehicles. It should be noted that a limitation to the reliability of this conclusion is the assumption of a similar proportion of volatile and non-volatile PN emissions for HEVs and conventional ICEs.

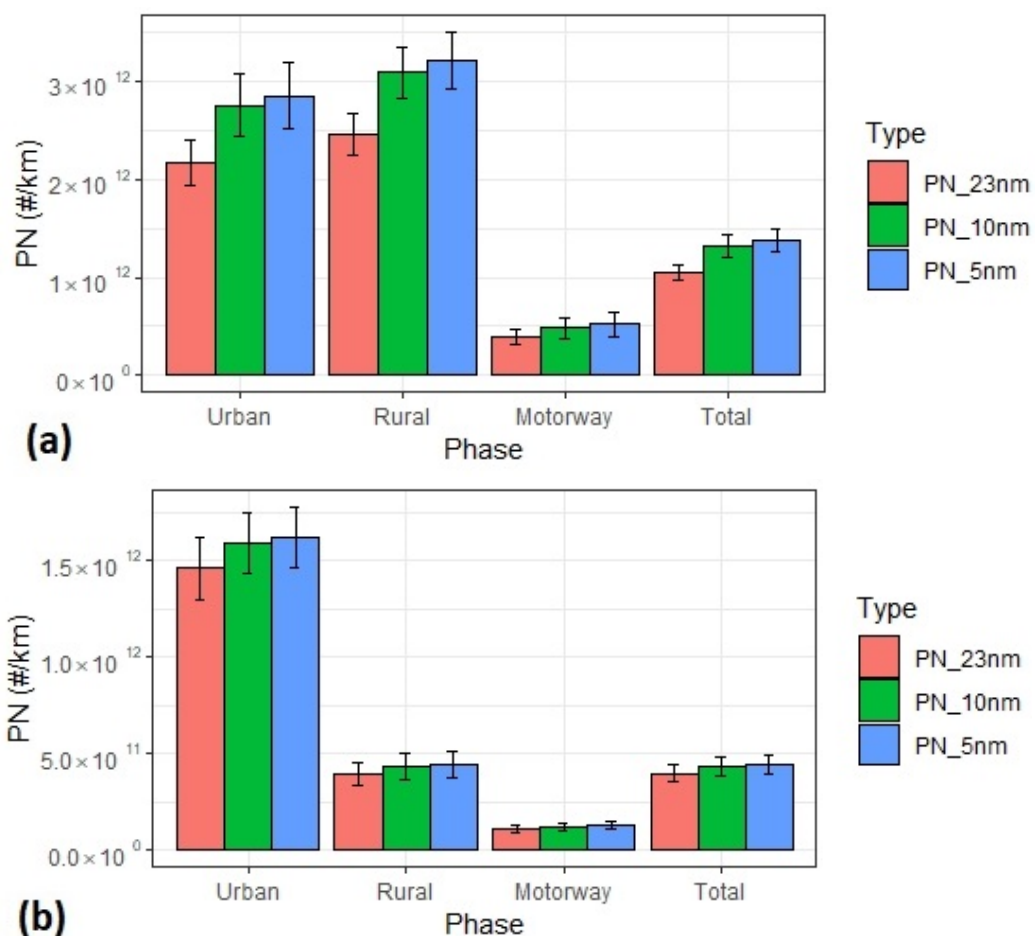


**Figure 20.** PN values comparing diameter cut-offs at 23 nm, 10 nm and 5 nm, across sections of (a) the WLTC and (b) the shortened RDE-style cycles. Error bars represent the standard error of the repeats (two tests for each WLTC phase, three tests for each RDE phase).

#### 4. Conclusions

This paper has studied the effects of drive cycle properties on the engine behaviour of an HEV and investigated how this impacts the tailpipe PN emissions and their PNSD. The number of vehicle stops has a large impact on increasing the reported PN emission factors. The overall PN emission factors for both RDE and WLTC testing are  $7.3 \times 10^{11}$  #/km and  $1 \times 10^{12}$  #/km, respectively; above the Euro 6 limit ( $6 \times 10^{11}$  #/km) for this HEV (note, however that this is a Euro 5 HEV). The urban section of the RDE test gave an emission factor of  $1.8 \times 10^{12}$  #/km; above the current RDE not-to-exceed (NTE) limit ( $9 \times 10^{11}$  #/km). These trends support the findings of Yang et al. [4] and indicate that HEV PN emissions should be more carefully monitored and considered in future regulations.

Building on the work of Conger and Holmén [26], the percentage proportions of PN emitted over the WLTC and an RDE-style drive cycle occupied by different HEV operating states were calculated. It was shown that the number of vehicle stops during a test cycle has a direct impact on the re-ignition activity for the HEV.  $64 \pm 3\%$  of total PN for WLTC and  $77 \pm 4\%$  of total PN for RDE were produced during engine re-ignition events and a further 30% and 13% were produced during other types of destabilised engine operation, for WLTC and RDE, respectively. Meanwhile,  $6 \pm 1\%$  and  $10 \pm 3\%$  was from stabilised engine operation for WLTC and RDE respectively. The majority of engine re-ignition and destabilised activity, and hence PN emissions, were found to occur during the low-speed urban and suburban sections of the drive cycles used. This highlights the importance of regulating HEV PN emissions in order to limit human exposure to PN.

For the first time in available literature, the PNSD arising from an HEV on WLTC and RDE cycles has been investigated, including the specific study of the differences in PNSD during engine re-ignition events compared to stable engine operation. The average PNSD across cycle phases was markedly different for the RDE compared to the WLTC. This variation was found to be due to the different PN emission behaviour seen under different types of engine operation, which was heavily influenced by the dynamic properties of the cycles under study. A merged wide peak with a maximum at 60 nm diameter and a shoulder at 12 nm diameter was seen for engine re-ignition and engine destabilised events. These PN emissions were shown to be due to fuel enrichment, in agreement with Conger and Holmén [26]. The stabilised engine state was associated with a tri-modal PNSD: There were low but almost constant magnitude PN emissions at 12 nm and 115 nm modes, and intermittent high magnitude peaks at 35 nm associated with sudden increases in engine speed. The study of the PNSD during warm and cold operation shows for the first time that this HEV has increased emissions of the 12 nm mode particles under a cold start, but similar overall PN emission values, compared to a warm start. The cut-off size at 23 nm by the PMP means that the reported PN emissions by legislation are underestimates. The impact of the 23 nm cut-off on reported WLTC PN emission factors was investigated for the HEV under study. Decreasing the cut-off from 23 nm to 10 nm was found to increase reported PN by 25% on the WLTC while decreasing to 5 nm increased reported PN by 31%. These differences are much smaller than those witnessed by Giechaskiel et al. [28] for two conventional PFI SI vehicles on the NEDC and WLTC, but still indicate that much of the PN is missed with a cut-off at 23 nm. Most of this HEV PN emissions would be captured if the cut-off were reduced to 10 nm.

The results of this work highlight the importance of controlling and regulating HEV PN emissions to limit human exposure to PN in urban environments where the majority of PN emissions were shown to occur. The findings also demonstrate the high level of dependency that HEV PN emission factors have on the properties of the test drive cycle used, and hence the attention that policymakers need to give to ensure that test drive cycles are as representative of real-world driving as possible. The sensitivity of HEV PNSD to engine behaviour and, in turn, to test cycle dynamic properties, is important to note when considering legislative test cycles, particularly with reference to the freedoms afforded by the RDE test cycle. The results also indicate that substantial improvements to air quality could be made by reducing the PMP PN cut-off to 10 nm.

**Author Contributions:** Conceptualisation, D.T. and H.L.; methodology, D.T. and H.L.; software, D.T., X.W. and K.R.; validation, D.T., X.W. and H.L.; formal analysis, D.T.; investigation, D.T. and X.W.; resources, H.L., C.D.B. and G.H.; data curation, D.T. and K.R.; writing—original draft preparation, D.T.; writing—review and editing, H.L., X.W., K.R. and A.S.T.; visualisation, D.T.; supervision, H.L.; project administration, D.T. and H.L.; funding acquisition, D.T. All authors have read and agreed to the published version of the manuscript.

**Funding:** Daisy Thomas would like to thank the Engineering and Physical Sciences Research Council (EPSRC) for a PhD studentship in the Centre for Doctoral Training in Bioenergy (EP/L014912/1). Hu Li and Xin Wang thank the Royal Society for an award “Investigating impact of E10 gasoline and its compositions on real driving emissions from in-service gasoline and hybrid vehicles” (IEC\NSFC\191747—International Exchanges 2019 Cost Share (NSFC)) in support of this work.

**Institutional Review Board Statement:** Not applicable.

**Informed Consent Statement:** Not applicable.

**Data Availability Statement:** The data presented in this study may be available on request from the corresponding author.

**Acknowledgments:** This research was possible due to the financial aid of the Engineering and Physical Sciences Research Council (EPSRC) for a PhD studentship for Daisy Thomas in the Centre for Doctoral Training in Bioenergy (EP/L014912/1). Thanks go to the technician Scott Prichard in the School of Chemical and Process Engineering for his help in the instrumentation and maintenance of

the research vehicle. We would also like to thank the University of Bath and Horiba UK for providing the Chassis testing facilities and PEMS (Portable Emission Measurement System), respectively.

**Conflicts of Interest:** The authors declare no conflict of interest.

## References

1. Vu, T.V.; Delgado-Saborit, J.M.; Harrison, R.M. Review: Particle Number Size Distributions from Seven Major Sources and Implications for Source Apportionment Studies. *Atmos. Environ.* **2015**, *122*, 114–132. [CrossRef]
2. Li, T.; Chen, X.; Yan, Z. Comparison of Fine Particles Emissions of Light-Duty Gasoline Vehicles from Chassis Dynamometer Tests and on-Road Measurements. *Atmos. Environ.* **2013**, *68*, 82–91. [CrossRef]
3. Karjalainen, P.; Pirjola, L.; Heikkilä, J.; Lähde, T.; Tzamkiozis, T.; Ntziachristos, L.; Keskinen, J.; Rönkkö, T. Exhaust Particles of Modern Gasoline Vehicles: A Laboratory and an on-Road Study. *Atmos. Environ.* **2014**, *97*, 262–270. [CrossRef]
4. Yang, Z.; Ge, Y.; Thomas, D.; Wang, X.; Su, S.; Li, H.; He, H. Real Driving Particle Number (PN) Emissions from China-6 Compliant PFI and GDI Hybrid Electrical Vehicles. *Atmos. Environ.* **2019**, *199*, 70–79. [CrossRef]
5. Eastwood, P. *Particulate Emissions from Vehicles*; John Wiley & Sons: Chichester, UK, 2008; ISBN 978-0-470-72455-2.
6. Raza, M.; Chen, L.; Leach, F.; Ding, S. A Review of Particulate Number (PN) Emissions from Gasoline Direct Injection (GDI) Engines and Their Control Techniques. *Energies* **2018**, *11*, 1417. [CrossRef]
7. Nose, H.; Inoue, T.; Katagiri, S.; Sakai, A.; Kawasaki, T.; Okamura, M. Fuel Enrichment Control System by Catalyst Temperature Estimation to Enable Frequent Stoichiometric Operation at High Engine Speed/Load Condition. *SAE Tech. Pap.* **2013**, *2*. [CrossRef]
8. Andrews, G.E.; Xu, J.; Sale, T. Influence of Catalyst and Exhaust System on Particulate Deposition and Release from an IDI Diesel Passenger Car under Real World Driving. *SAE Tech. Pap.* **2002**. [CrossRef]
9. von Klot, S.; Peters, A.; Aalto, P.; Bellander, T.; Berglind, N.; D'Ippoliti, D.; Elosua, R.; Hörmann, A.; Kulmala, M.; Lanki, T.; et al. Ambient Air Pollution Is Associated with Increased Risk of Hospital Cardiac Readmissions of Myocardial Infarction Survivors in Five European Cities. *Circulation* **2005**, *112*, 3073–3079. [CrossRef]
10. Curtis, L.; Rea, W.; Smith-Willis, P.; Fenyves, E.; Pan, Y. Adverse Health Effects of Outdoor Air Pollutants. *Environ. Int.* **2006**, *32*, 815–830. [CrossRef]
11. Uherek, E.; Halenka, T.; Borken-Kleefeld, J.; Balkanski, Y.; Berntsen, T.; Borrego, C.; Gauss, M.; Hoor, P.; Juda-Rezler, K.; Lelieveld, J.; et al. Transport Impacts on Atmosphere and Climate: Land Transport. *Atmos. Environ.* **2010**, *44*, 4772–4816. [CrossRef]
12. Myung, C.L.; Park, S. Exhaust Nanoparticle Emissions from Internal Combustion Engines: A Review. *Int. J. Automot. Technol.* **2012**, *13*, 9–22. [CrossRef]
13. Oberdörster, G. Significance of Particle Parameters in the Evaluation of Exposure-Dose Response Relationships of Inhaled Particles. *Part. Sci. Technol.* **1996**, *14*, 135–151. [CrossRef]
14. Donaldson, K.; Li, X.Y.; MacNee, W. Ultrafine (Nanometre) Particle Mediated Lung Injury. *J. Aerosol Sci.* **1998**, *29*, 553–560. [CrossRef]
15. Samaras, Z.C.; Andersson, J.; Bergmann, A.; Hausberger, S.; Toumasatos, Z.; Keskinen, J.; Haisch, C.; Kontses, A.; Ntziachristos, L.D.; Landl, L.; et al. Measuring Automotive Exhaust Particles Down to 10 nm. 2020. Available online: <https://trepo.tuni.fi/handle/10024/136321> (accessed on 2 June 2022).
16. Giechaskiel, B.; Maricq, M.; Ntziachristos, L.; Dardiotis, C.; Wang, X.; Axmann, H.; Bergmann, A.; Schindler, W. Review of Motor Vehicle Particulate Emissions Sampling and Measurement: From Smoke and Filter Mass to Particle Number. *J. Aerosol Sci.* **2014**, *48*–86. [CrossRef]
17. Otsuki, Y.; Nakamura, H.; Arai, M.; Xu, M. The Methodologies and Instruments of Vehicle Particulate Emission Measurement for Current and Future Legislative Regulations. *Meas. Sci. Technol.* **2015**, *26*, 092002. [CrossRef]
18. Christenson, M.; Loiselle, A.; Karman, D.; Graham, L.A. The Effect of Driving Conditions and Ambient Temperature on Light Duty Gasoline-Electric Hybrid Vehicles (2): Fuel Consumption and Gaseous Pollutant Emission Rates. *SAE Tech. Pap.* **2007**. Available online: <https://www.sae.org/publications/technical-papers/content/2007-01-2137/> (accessed on 2 June 2022).
19. Robinson, M.K.; Holmén, B.A. Onboard, Real-World Second-by-Second Particle Number Emissions from 2010 Hybrid and Comparable Conventional Vehicles. *J. Transp. Res. Board* **2011**, *2233*, 63–71. [CrossRef]
20. Wei, Q.; Porter, S. Evaluation of Solid Particle Emissions from Hybrid and Conventional Gasoline Vehicles. *SAE Int. J. Engines* **2011**, *4*, 619–638. [CrossRef]
21. Kontses, A.; Triantafyllopoulos, G.; Ntziachristos, L.; Samaras, Z. Particle Number (PN) Emissions from Gasoline, Diesel, LPG, CNG and Hybrid-Electric Light-Duty Vehicles under Real-World Driving Conditions. *Atmos. Environ.* **2020**, *222*, 117126. [CrossRef]
22. Marotta, A.; Pavlovic, J.; Ciuffo, B.; Serra, S.; Fontaras, G. Gaseous Emissions from Light-Duty Vehicles: Moving from NEDC to the New WLTP Test Procedure. *Environ. Sci. Technol.* **2015**, *49*, 8315–8322. [CrossRef]
23. Johnson, T.V. Vehicular Emissions in Review. *SAE Int. J. Engines* **2016**, *9*, 1258–1275. [CrossRef]
24. Thomas, D.; Li, H.; Ropkins, K.; Wang, X.; Ge, Y. Investigating the Engine Behavior of a Hybrid Vehicle and Its Impact on Regulated Emissions during On-Road Testing. *SAE Tech. Pap.* **2019**. [CrossRef]
25. Commission Regulation (EU) 2017/1151 of 1 June 2017. *Off. J. Eur. Union* **2017**, L 175. Available online: <https://eur-lex.europa.eu/legal-content/EN/TXT/?uri=celex%3A32017R1151> (accessed on 2 June 2022).

26. Conger, M.; Holmén, B.A. Characterization of Real-World Particle Number Emissions during Reignition Events from a 2010 Light-Duty Hybrid Electric Vehicle. *Transp. Res. Rec. J. Transp. Res. Board* **2015**, *2503*, 137–146. [[CrossRef](#)]
27. Premnath, V.; Khalek, I.; Morgan, P.; Michlberger, A.; Sutton, M.; Vincent, P. Effect of Lubricant Oil on Particle Emissions from a Gasoline Direct Injection Light-Duty Vehicle. *SAE Tech. Pap.* **2018**. Available online: <https://www.sae.org/publications/technical-papers/content/2018-01-1708/> (accessed on 2 June 2022).
28. Giechaskiel, B.; Vanhanen, J.; Väkevä, M.; Martini, G. Investigation of Vehicle Exhaust Sub-23 nm Particle Emissions. *Aerosol Sci. Technol.* **2017**, *51*, 626–641. [[CrossRef](#)]